Factors Influencing Optic Nerve Head Biomechanics

Ian A. Sigal,[1,2] John G. Flanagan,[3,4] and C. Ross Ethier[1,2,3]

PURPOSE. The biomechanical environment within the optic nerve head (ONH) may play a role in retinal ganglion cell loss in glaucomatous optic neuropathy. This was a systematic analysis in which finite element methods were used to determine which anatomic and biomechanical factors most influenced the biomechanical response of the ONH to acute changes in IOP.

METHODS. Based on a previously described computational model of the eye, each of 21 input factors, representing the biomechanical properties of relevant ocular tissues, the IOP, and 14 geometric factors were independently varied. The biomechanical response of the ONH tissues was quantified through a set of 29 outcome measures, including peak and mean stress and strain within each tissue, and measures of geometric changes in ONH tissues. Input factors were ranked according to their aggregated influence on groups of outcome measures.

RESULTS. The five input factors that had the largest influence across all outcome measures were, in ranked order: stiffness of the sclera, radius of the eye, stiffness of the lamina cribrosa, IOP, and thickness of the scleral shell. The five least influential factors were, in reverse ranked order: retinal thickness, peripapillary rim height, cup depth, cup-to-disc ratio, and pial thickness. Factor ranks were similar for various outcome measure groups and factor ranges.

CONCLUSIONS. The model predicts that ONH biomechanics are strongly dependent on scleral biomechanical properties. Acute deformations of ONH tissues, and the consequent high levels of neural tissue strain, were less strongly dependent on the action of IOP directly on the internal surface of the ONH than on the indirect effects of IOP on the sclera. This suggests that interindividual variations in scleral properties could be a risk factor for the development of glaucoma. Eye size and lamina cribrosa biomechanical properties also have a strong influence on ONH biomechanics. (*Invest Ophthalmol Vis Sci.* 2005;46: 4189–4199) DOI:10.1167/iovs.05-0541

Elevated intraocular pressure (IOP) is the primary risk factor for the development of glaucomatous optic neuropathy. The mechanism whereby IOP induces loss of retinal ganglion cell function in glaucoma is not well understood, but has been postulated to involve both biomechanical and vascular effects. Biomechanically, it is hypothesized that IOP-induced mechanical strain on glial cells supporting ganglion cell axons eventually leads to apoptosis of the ganglion cells and the consequent loss of vision.[1–3] However, the "safe" level of IOP is patient specific,[4] a difference that is likely due, at least in part, to differences in optic nerve head (ONH) geometry and biomechanical properties. An improved understanding of the ONH biomechanical environment, and of the dependence of this environment on the geometry and biomechanical properties of the ONH tissues, is necessary to understand better how biomechanical effects may play a role in glaucomatous optic neuropathy.

Unfortunately, direct measurement of the ONH biomechanical environment is not possible at present, and alternate approaches are therefore needed. One such approach is modeling. Initial models were mathematical and had several limitations (discussed in Ref. 5). More recently, computational models based on the finite element approach have been able to overcome some of these limitations. For example, studies using a simplified (generic) ONH shape can match the general magnitude and shape of observed vitreoretinal interface deformations due to changes in IOP[5] and have highlighted how scleral canal shape can affect ONH biomechanics.[6] More sophisticated individual-specific models are now being developed, reproducing in detail the anatomy of an individual optic nerve head in monkeys[7] and humans.[8]

The numerical modeling process involves assumptions and simplifications whose effects must be carefully considered in interpreting model results. For example, it is necessary to assign biomechanical property values (e.g., stiffness, compressibility) to ONH tissues, but reported data for these properties show a large range,[5] likely reflecting interindividual differences and aging effects. Moreover, models based on a "generic" ONH geometry make assumptions about which tissue components to consider and their shape. Individual-specific models reduce the arbitrary geometric nature of generic models, but still make important assumptions about which tissue components to consider, the level of detail in modeling, the size of the region to model, and material properties.

To guide future modeling and experimental studies, it would be helpful to understand how sensitive model predictions are to these assumptions and simplifications. In this regard, it is useful to think of the computational modeling process as a black box with a set of inputs (e.g., tissue geometry and tissue mechanical properties) that produces a set of outcome measures (e.g., mechanical strain on lamina cribrosa [LC] tissues). Our goal in this work was to define the sensitivity of model outcome measures to variations in model inputs.

One complication of such a sensitivity analysis is that there is no model outcome measure that is universally accepted for predicting the risk of glaucomatous optic neuropathy. We will therefore look at a variety of model outcome measures, selected either because they are clinically observable (e.g., shape of the cup) or because there is a reasonable chance that they are biologically significant in the pathogenesis of glaucomatous optic neuropathy (e.g., strain in the LC). This complicates the analysis; nonetheless, we shall see that certain inputs have a consistently large effect on many of the outcome measures,

TABLE 1. Input Factors and Their Baseline Values and Ranges Used in the Sensitivity Analysis (see Figure 1 for Factor Definitions)

Name	Coded Name	Units	Baseline	Low	High	Sources
Input factors defining the geometry of the eye and ONH						
Internal radius of eye shell	EyeRadius	mm	12.0	9.6	14.4	9–13
Scleral thickness at canal	ScThickAtCanal	mm	0.4	0.32	0.48	13–16
Laminar thickness at axis	LCThickAxis	mm	0.3	0.24	0.36	13,16–18
Retinal thickness	RetThickShell	mm	0.2	0.16	0.24	19,20
Scleral shell thickness	ScThickShell	mm	0.8	0.64	0.96	11,14,15
LC anterior surface radius	LCRadius	mm	0.95	0.76	1.14	10,12,13,16,18,21–24
Pia mater thickness	PiaThick	mm	0.06	0.048	0.072	13
Laminar curvature	LCDepth	mm	0.2	0	0.2	*
Cup-to-disc ratio/shape of the cup	Cup2DiscRatio	—	0.25	0.1	0.5	19,21
Canal wall angle to the horizontal	AngleScCanal	deg	60	48	72	*
Optic nerve angle	AngleON	deg	80	64	96	*
Scleral thinning/peripapillary scleral tapering	ScThinFactor	—	0.5	0	1.0	11,15
Peripapillary rim height	RimHeight	mm	0.3	0.24	0.36	19,21,25
Cup depth	CupDepth	mm	0.33	0.26	0.4	19,21
Input factors defining the load on ONH tissues						
Intraocular pressure	IOP	mm Hg	25	20	30	26,27
Input factors defining the biomechanical properties of relevant optic tissues						
Poisson ratio of retina	RetPoisson	—	0.49	0.4	0.49	28–30
Pia mater Young's modulus	PiaModulus	MPa	3	1	9	31–33
Lamina cribrosa Young's modulus	LCModulus	MPa	0.3	0.1	0.9	6,34–36
Sclera Young's modulus	ScModulus	MPa	3	1	9	29,37–44,54
Retina Young's modulus	RetModulus	MPa	0.03	0.01	0.09	45–50
Optic nerve Young's modulus	ONModulus	MPa	0.03	0.01	0.09	Same as for retina

Ranges were estimated from our own measurements (*), or from a combination of our measurements and the sources listed (see the Methods section for details). In many cases, the sources did not directly measure the quantity of interest. In such situations, we computed the quantity of interest from the data that were reported.

making us confident that such inputs are biomechanically important.

METHODS

Our general approach was to define a baseline model of the ONH. We then identified 21 input factors that determined the geometry, material properties and IOP of the model, and systematically varied each input factor to determine how the input factors influenced the outcome measures. The effect of each factor was investigated separately (i.e., when one factor was varied, all other factors were kept at their baseline values).

The Baseline Model

The sensitivity analysis was carried out based on a previously described model.[5] Briefly, the model was axisymmetric and consisted of five tissue regions: corneoscleral shell, LC, prelaminar neural tissue (including the retina), and postlaminar neural tissue (including the optic nerve), and pia mater. The ONH was modeled in some detail, whereas the rest of the eye was modeled as a spherical shell of constant thickness. For the study presented herein, we used a slightly modified form of Model 3 from our prior study,[5] in which the geometry of the region where the pia mater meets the sclera was simplified, with the intention of reducing artifactual concentrations of stress and strain, and preventing the occurrence of computationally inefficient (and possibly inaccurate) high-aspect ratio elements. As before, all tissues were assumed to be linearly elastic and isotropic, with their mechanical behavior determined by their Young's modulus and Poisson ratio.

Input Factors

The input factors, along with their baseline values and ranges, are listed in Table 1 and are shown in Figure 1. It is convenient to subdivide the input factors into three categories.

Tissue Material Properties. These include Young's modulus (stiffness) for each of the five tissue regions and the compressibility (Poisson ratio) of the prelaminar neural tissues, since it has been

suggested that the prelaminar neural tissues could change their volume with IOP.[1,51] We assumed that all tissues were linearly elastic and isotropic and that all tissues except for the prelaminar neural tissues were incompressible.

Tissue Loading. IOP has been identified as the principal risk factor for the development of glaucomatous optic neuropathy. Consequently, we included this boundary condition as an input factor, allowing us to evaluate the magnitude of its effects relative to those of other factors.

Geometry of the Ocular Tissues. There is some arbitrariness in how the ocular geometry was specified. We defined 14 geometric factors that together spanned a wide range of possible globe sizes and ONH shapes (see Fig. 1 for definitions). These geometric input factors included the thickness of the prelaminar neural tissue, LC, pia mater, and sclera at different points; the shapes of the scleral canal and optic cup; the eye globe radius and thickness; the curvature of the LC; and the shape of the peripapillary sclera. Herein, we give notes explaining how some of these factors were defined. The scleral point closest to the axis of symmetry was defined as the scleral tip, and its distance to the axis of symmetry as the radius of the scleral canal. Directly anterior (i.e., on a line parallel to the axis of symmetry) to the tip of the sclera, at a distance defined as rim height, was the retinal rim top. From the retinal rim top, away from the axis of symmetry, the prelaminar neural tissue thinned smoothly, attaining the retina shell thickness at a point that represented the rim perimeter. Orthogonal to the axis of symmetry, we defined a reference level 50 μm posterior to the rim perimeter (Fig. 1; dashed line), representing the scanning laser tomograph's reference plane (Heidelberg Retina Tomograph; Heidelberg Engineering, Heidelberg, Germany).[25] The shape of the cup was characterized by a cup-to-disc ratio, as measured at this reference level. The shape of the cup varied from a relatively small cup with steep walls (cup-to-disc ratio of 0.1) to a relatively large, flat cup (cup-to-disc ratio of 0.5). Cup depth was defined as the distance from the bottom of the cup to the reference level. We varied the curvature of the LC by changing the depth of the anterior LC surface at the axis of symmetry with respect to the same surface at the edge of the LC. As this depth increases, the LC shape varies from flat (depth 0) to more curved. The shape of the
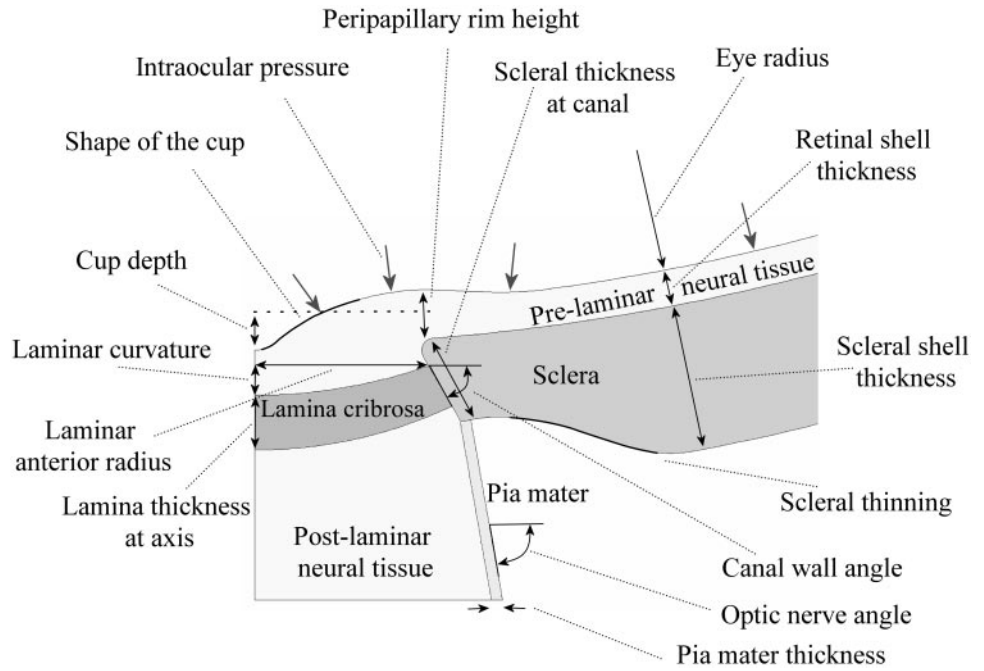
FIGURE 1. Input factor definitions superimposed on the baseline model geometry (only the ONH region of the entire eye is shown). See Table 1 for input factor ranges. In addition to the input factors shown, the compressibility (Poisson ratio) of the prelaminar neural tissue and the stiffness (Young's modulus) of each tissue region, were varied, for a total of 21 input factors. *Dashed line*: a reference level used to compute cup-to-disc ratio and cup depth. The illustration represents the model geometry at a pressure of 0 mm Hg.

posterior peripapillary sclera was parameterized and varied from 0 to 1, representing variations with little to significant scleral thinning. The optic nerve and canal wall angles are related to parameters identified by Burgoyne et al.[7] that help determine the thickness of the peripapillary sclera—namely, the angle of the neural canal wall and the oblique orientation of the canal's passage through the sclera. In our models, which are asymmetric, these input factors measured the rate of enlargement of the canal diameter and retrobulbar optic nerve.

For each input factor, the baseline value and range of admissible values were defined from the literature, when available, or from our own estimates, based on measurements on serial sections of the ONH from ostensibly healthy donor human eyes.[8] For a number of input factors the range of physiologically reasonable values is unknown. An unnaturally large range could make a factor artificially influential and conversely make other factors artificially modest. We therefore tried to reduce the arbitrariness of the input factor ranges by varying input factors over comparable ranges. Specifically, all tissue stiffnesses (Young's moduli) were varied from one-third to three times the values in the baseline model, which is within the range of reported experimental values. The prelaminar tissue Poisson ratio varied from practically incompressible ($\nu = 0.49$) to relatively low ($\nu = 0.4$). Many geometric factors were varied in the range ±20% around the values of the baseline model.

In addition, we evaluated the possible effects of input factor ranges by repeating the study under three conditions: full factor ranges, as described earlier, halved factor ranges (for all factors, except IOP), and minimal factor ranges defined as one twenty-fourth of the full range. The advantage of using smaller input factor ranges is that it allows us to minimize nonlinear effects that are seen in some outcome measures, as will be described in the following sections.

Numerical Details

The construction of the model geometry was scripted so that a set of parameters defining the input factors could be read from a file and a model generated, solved, and analyzed automatically within a finite element package (ANSYS, ver. 8; ANSYS Inc., Canonsburg, PA) in a few seconds using a desktop workstation. All models were meshed with eight-node quadrilateral elements (Plane82), using the finite element's own automated meshing routines. In a preliminary study,[5] a mesh refinement analysis was performed based on the structural percentage error in energy norm (SEPC), a measure of the discontinuity of the stresses, sequentially refining the baseline model until the SEPC mea-

sure dropped below 1%. The resultant element size was halved and used as the target element size when meshing each of the models in the study. If during the parametric analysis a model predicted particularly large stress or strain levels, its SEPC value was checked to confirm that it was below 1%. There was never a need to remesh a model to guarantee a converged solution.

Finite element simulations were carried out for 25 equally spaced values of each input factor within its given range, giving a total of 505 models (21 factors, each at 25 levels, minus the 20 repetitions of the baseline model of each factor). Thirteen equally spaced values for each input factor were used for the half-range conditions (253 models) and two values for the minimal range conditions (22 models). Postprocessing analyses were performed on computer (Excel 2003; Microsoft Corp., Redmond, WA).

Outcome Measures

Several different outcome measures are possible, and the choice of these measures was motivated by what we believe is biologically important or clinically observable. We chose 29 outcome measures (Table 2), divided into the following categories.

Strain and Stress. Strain represents the amount of stretching that a tissue undergoes, and stress is the force within the tissue per unit of tissue area. Strain is important since most research in mechanobiology suggests that cells respond to strain (deformation) rather than directly to stress. Stress is important because it determines the tendency of extracellular materials to fail (tear) as occurs at the periphery of the glaucomatous LC.[1] It is important to differentiate between stress and strain when evaluating mechanical effects on cells and tissues, which is why we have considered both of these quantities. Unfortunately, strain and stress are tensor quantities that cannot be completely specified by a single value at a given location. For this work, we chose the maximum principal strain as a measure of maximum tissue strain and von Mises stress as a measure of stress.[52] Assuming isotropic linearly elastic tissue, all stresses and strains scale linearly with the applied loads. Therefore, we report stresses as multiples of the baseline IOP (25 mm Hg).

We tracked the maximum principal strain and von Mises stress within each of the five tissue regions, computing mean and peak values within each region. Peak values of strain (stress) were defined as the average of the strain (stress) values in the 5% of the tissue volume having the largest strain (stress). This definition minimizes the effects

TABLE 2. Outcome Measures Used in the Sensitivity Analysis

Outcome Measure	Code	Units	Min	Max
Outcome measures related to mechanical stress and strain in ONH tissues				
Peak maximum principal strain				
Retina	RetE5	%	1.94	6.19
Lamina cribrosa	LcE5	%	1.89	7.94
Optic nerve	OnE5	%	2.12	9.68
Sclera	ScE5	%	0.74	4.48
Pia mater	PiaE5	%	1.07	5.01
Peak von Mises stress				
Retina	RetS5	kPa	0.62	4.04
Lamina cribrosa	LcS5	kPa	7.35	45.24
Optic nerve	OnS5	kPa	0.70	5.30
Sclera	ScS5	kPa	49.04	74.17
Pia mater	PiaS5	kPa	43.28	232.57
Mean maximum principal strain				
Retina	RetE100	%	0.54	2.77
Lamina cribrosa	LcE100	%	1.53	5.30
Optic nerve	OnE100	%	1.04	2.50
Sclera	ScE100	%	0.33	2.42
Pia mater	PiaE100	%	0.29	1.04
Mean von Mises stress				
Retina	RetS100	kPa	0.28	1.48
Lamina cribrosa	LcS100	kPa	6.50	30.67
Optic nerve	OnS100	kPa	0.25	1.59
Sclera	ScS100	kPa	28.61	42.92
Pia mater	PiaS100	kPa	7.91	48.73
Outcome measures related to ONH geometry				
Retinal thickness at axis of symmetry	RetThickAxis	μm	-26.1	-3.05
Retinal thickness midway from axis to canal rim	RetThickMidway	μm	7.1	41.0
Radius of scleral canal at opening	CanalRadius	μm	5.24	38.8
Cup-to-disc ratio	CupToDiscRatio		0.00	0.02
Lamina cribrosa thickness at axis of symmetry	LcThickAxis	μm	-24.4	-8.38
Lamina cribrosa thickness midway from axis to rim	LcThickMidway	μm	-25.5	-7.7
Lamina cribrosa thickness at rim	LcThickRim	μm	-10.5	-1.36
Angle to the horizontal of scleral canal wall	AngleScCanal	deg	-5.27	-1.3
Bottom of cup depth from HRT level	CupDepth	μm	-14.3	0.11

The numbers in the final two columns are the minimum and maximum value for the change in each outcome measure computed over all simulations (i.e. over all variations of the input factors). For purposes of computing the change, the reference state was defined to be the condition of IOP = 0. Therefore, a negative number in the last two columns means that the geometric outcome measure value decreased as the IOP was increased. A pressure of 25 mm Hg corresponds to 33.33 kPa.

of outliers in the strain (stress) distribution that could depend on the specifics of the numerical discretization or on outliers from regions too small to have physiologic significance. Peak and mean values of maximum principal strain and von Mises stress for each of the five tissue regions produce 20 outcome measures for each model configuration.

Geometric Changes. We defined nine geometric features as outcome measures (see Table 2 and Fig. 2). These included: scleral canal radius, as described in the section on input factors; thickness of the prelaminar neural tissue and the LC, measured at the axis of symmetry and halfway between the axis and the same tip of the sclera used for the canal radius, LC thickness at the scleral canal wall, and the angle of the scleral canal wall with respect to a line orthogonal to the axis of symmetry. Finally, cup depth and cup-to-disc ratio were computed in the same way as in the definition of the input factors, but based on a reference level updated for the deformed geometry.

In total 14,645 outcome measures were computed (29 measures for each of 505 models). With so much data, it was essential to have a rational and systematic way to analyze the information, and to this end we adopted the following approach. We first asked: How much does a single outcome measure vary as a single input factor varies over its range? To answer this question we defined the **absolute response** of an outcome measure to a single input factor as the range (maximum − minimum) of the outcome measure values while varying only that input factor. Therefore, there is one absolute response number for every pairing of input factor and outcome measure. For each outcome measure, we then summed the absolute responses of all input factors to obtain the outcome measure **total response**, and then quantified

the influence of a single input factor, a **relative response**, as the percentage of this total response. The relative response therefore quantifies the relative importance of a single input factor for only one outcome measure. A more global view is obtained by adding the relative responses of a single input factor over a set of outcome measures. This was defined as the input factor's **total influence**.

For the condition of minimal factor ranges, an outcome measure's absolute response is akin to the slope, or rate of change, of the outcome measure as a function of the input factor, reinforcing the idea of this condition as a local analysis.

Input factors were ranked according to their total influence. Because we are not certain which outcome measure correlates most strongly with the development of glaucomatous optic neuropathy, we repeated this ranking using various groupings, or sets, of outcome measures. Four groups were formed by each of peak and mean strain and peak and mean stress within all five tissue regions. Outcome measures related to ONH geometry were divided grossly according to how easily they can be observed in a clinical setting into observable (cup-to-disc ratio, cup depth, and scleral canal radius), and nonobservable (retinal and laminar thicknesses and angle of scleral canal wall).

RESULTS

To illustrate the effects of a single input factor, Figure 3 shows how the maximum principal strain field in the ONH changed as scleral stiffness was varied. A steep line in the top panel
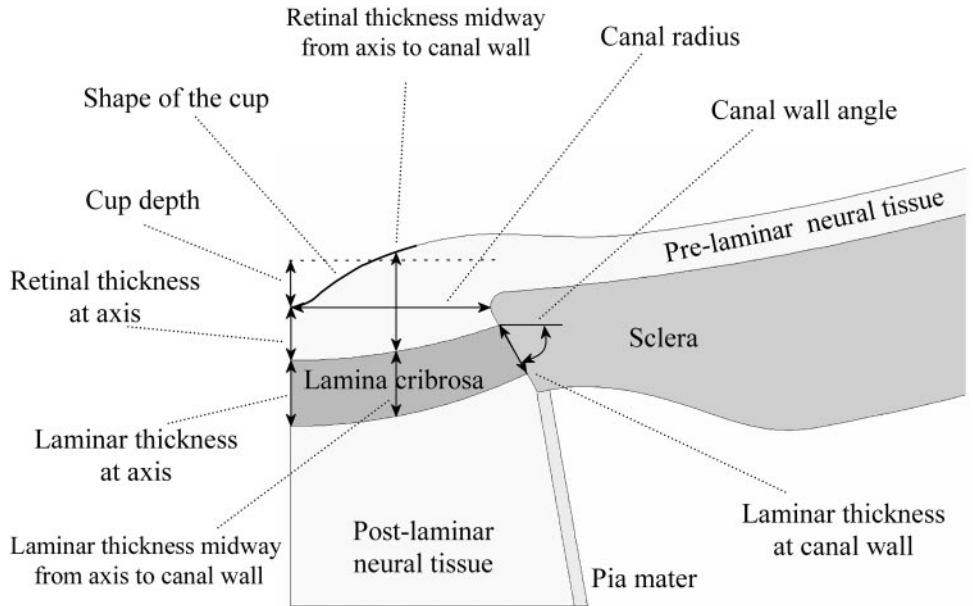
Figure 2. Definitions of geometric features, whose changes are used as outcome measures, superimposed on the baseline model geometry (only ONH region of entire eye is shown). In addition to the geometric outcome measures shown we also computed peak and mean maximum principal strain and peak and mean von Mises stress within each of the tissue regions, for a total of 29 outcome measures. *Dashed line:* a reference level used to compute cup depth and cup-to-disc ratio.

indicates that scleral stiffness had a large effect on the outcome measure. Mean strain levels within the prelaminar neural tissue and LC decreased as the sclera stiffened, with larger effects occurring for more compliant (less stiff) scleras. However, peak strains did not show a monotonic decline. This occurred because the sclera near the termination of Bruch's membrane showed an increase in strain levels as the sclera stiffened (Fig. 3, contour plots), the opposite of the behavior of most of the ONH. The net effect was a minimum value in peak strain at intermediate scleral stiffnesses.

When interpreting contour plots such as those shown in the lower part of Figure 3, we must be careful to remember that we are seeing only a flat (two-dimensional) representation of a model with axial symmetry and that the volume subtended by different regions depends on their distance to the axis of symmetry and their shape. For example, identical regions close to the axis of symmetry subtend smaller volumes than those

farther away from this axis. Therefore, the relatively large strain concentrations near the bottom of the cup occur only in a small volume and have a limited effect on mean strain. Conversely, the lower strain levels in the prelaminar neural tissue away from the ONH and near the opening of the scleral canal occur in larger volumes, where small changes can have large effects on mean strain.

Considering all simulations, mean and peak maximum principal strains were highest within the neural and laminar regions, reaching potentially biologically significant levels greater than 5% within most optic nerve tissues (Table 2; rightmost column). The range of strain and stress variation was widest within scleral tissue. The data in Table 3 also provide information on how the ONH tissues deformed; for example, note that the prelaminar neural tissue thinned at the axis of symmetry and thickened midway from the axis to the canal rim, whereas laminar thickness always decreased.
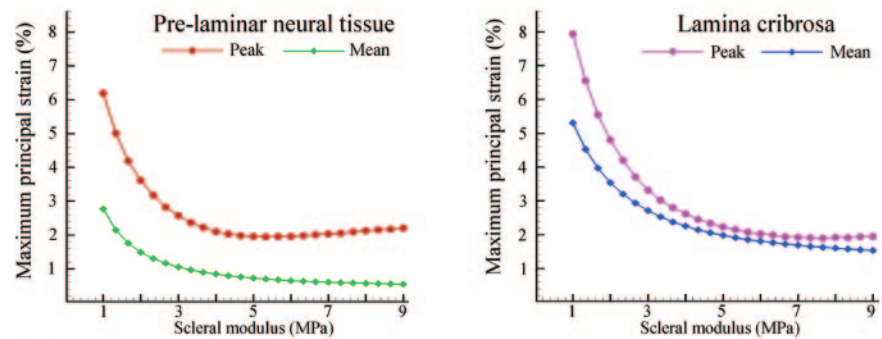

Figure 3. Effects of variations in scleral modulus on maximum principal strains in ONH tissues. *Top:* peak and mean maximum principal strain within the prelaminar neural tissue (*left*) and LC (*right*) as a function of scleral stiffness at an IOP of 25 mm Hg. *Bottom:* plots showing contours of maximum principal strain superimposed on the geometries of the model with deformations exaggerated five times, for three scleral modulus values.
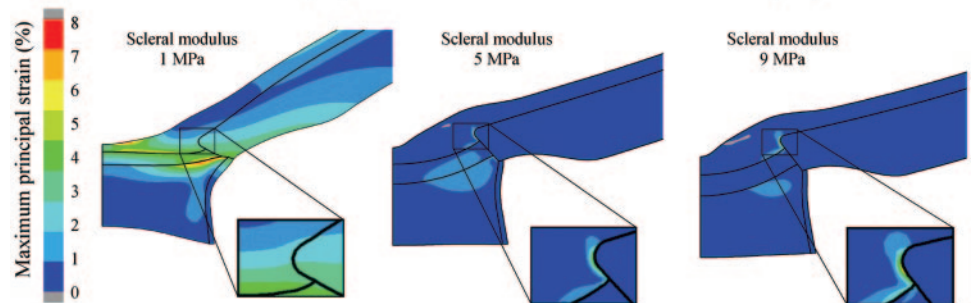
TABLE 3. Rankings of Input Factors as Determined by Sensitivity Analysis

Input Factor	All	Strain Peak	Strain Mean	Strain All	Stress Peak	Stress Mean	Stress All	Geometry Non-observable	Geometry Observable	Mean
Eye Radius	2	2	4	2	2	4	3	2	2	2.6
Scleral Canal Thickness	11	6	8	7	10	11	11	10	12	9.6
Lamina Thickness	14	12	11	12	14	13	14	7	17	12.7
Retina Thickness Shell	21	17	19	18	18	19	18	21	19	18.9
Sclera Thickness Shell	5	5	6	5	8	8	8	8	4	6.3
Lamina Width / Radius	6	9	5	6	11	10	9	6	3	7.2
Pia Thickness	17	14	15	15	16	17	17	18	21	16.7
Lamina Depth below rim	10	10	12	11	12	14	13	5	8	10.6
Cup to Disc ratio	18	19	20	20	19	20	20	17	7	17.8
Angle Scleral Canal Wall	15	15	14	14	15	15	15	13	14	14.4
Angle Optic Nerve	16	16	13	13	17	16	16	19	20	16.2
Sclera Thin Factor	13	8	10	9	9	12	12	12	15	11.1
Rim Height	20	21	18	19	20	18	19	20	18	19.2
Cup Depth	19	20	21	21	21	21	21	16	9	18.8
IOP	4	3	2	3	4	3	4	4	5	3.6
Ret Poisson ratio	12	18	17	17	13	9	10	9	6	12.3
Modulus Pia	7	7	9	8	5	5	5	14	16	8.4
Modulus Lamina	3	4	3	4	3	2	2	3	10	3.8
Modulus Sclera	1	1	1	1	1	1	1	1	1	1.0
Modulus Retina	9	13	16	16	7	7	7	11	11	10.8
Modulus Optic Nerve	8	11	7	10	6	6	6	15	13	9.1

A rank of 1 means that the input factor had the largest total influence (see text for definition of total influence), 2 means that the input factor had the second-largest total influence, and so forth. Cells are shaded green when the rank is within the top five, and orange when the rank is within the bottom five. Factor ranking depends on the set of outcome measures considered. Columns 2–10 represent different sets of outcome measures. Column 2 considers all outcome measures. The ranks in column 3 were computed using peak strains within all tissues as outcome measures. Column 4 contains similar rankings when considering mean strains. Column 5 considers both peak and mean strains. Columns 6–8 are similar, with stress replacing strain. Columns 9 and 10 consider only outcome measures related to model geometry (see text for definitions of groups). The numbers in column 10 are the mean rank averaged over all outcome measure sets (i.e., over columns 3–10). All ranks in this table were computed using input factor full ranges.

A more comprehensive view of the effects of multiple input factors on strain in the prelaminar neural tissue is shown in the top panel of Figure 4, which provides a visual representation of the relative importance of the various input factors. Most of the input factors had little effect (black lines), but scleral modulus clearly had a large effect (red line). Other input factors such as the radius of the globe, scleral thickness, IOP, and LC radius, had modest but nontrivial effects.

When we considered a different outcome measure, for example scleral canal radius (Fig. 4; bottom panel), scleral modulus still had the largest effect of all input factors. However, the ranking of the top five input factors changed slightly. This shows, as might be expected a priori, that different outcome measures have different sensitivities to the input factors. It is therefore important to look at a range of outcome measures to determine overall trends about which input factors are most important—a task to which we now turn.

The relative responses of all outcome measures to variations in all factors are shown in the left side of Figure 5. The details for each outcome measure are different, and therefore the overall influence of an input factor depends on the set of outcome measures that are examined. Despite this, several broad trends emerged. First, scleral modulus (orange bars near bottom) had a very substantial effect on almost every outcome measure. Other input factors, such as IOP, globe radius, and LC modulus, had a less striking effect that is nonetheless appreciable. In contrast, some input factors had consistently little or no effect, such as pial and retinal thicknesses. This is perhaps easier to appreciate on the right side of Figure 5, where we plotted total influences, obtained by summing relative responses for each input factor over all outcome measures. It can be seen that no matter what range of input values was used the five most influential factors were consistent and account for approximately two thirds of all outcome measure variations, with scleral modulus alone contributing approximately one third. In fact, narrower factor ranges had an even larger scleral modulus contribution. The five least influential factors were also only slightly affected by the range of input factors chosen, and accounted for only approximately 2% or 3% of all outcome measure variations.

The ranks of input factors according to their total influence are shown in Table 3. Columns correspond to input factor ranks computed with different outcome measure groups, or with different factor range conditions. When considering different columns, several consistent themes emerged. Most important, we concluded that scleral modulus was the most influential input factor for all outcome measure groups and factor range conditions. The IOP, modulus of the LC, and radius of the globe were also consistently influential. Confidence in the robustness of the results is enhanced by noting
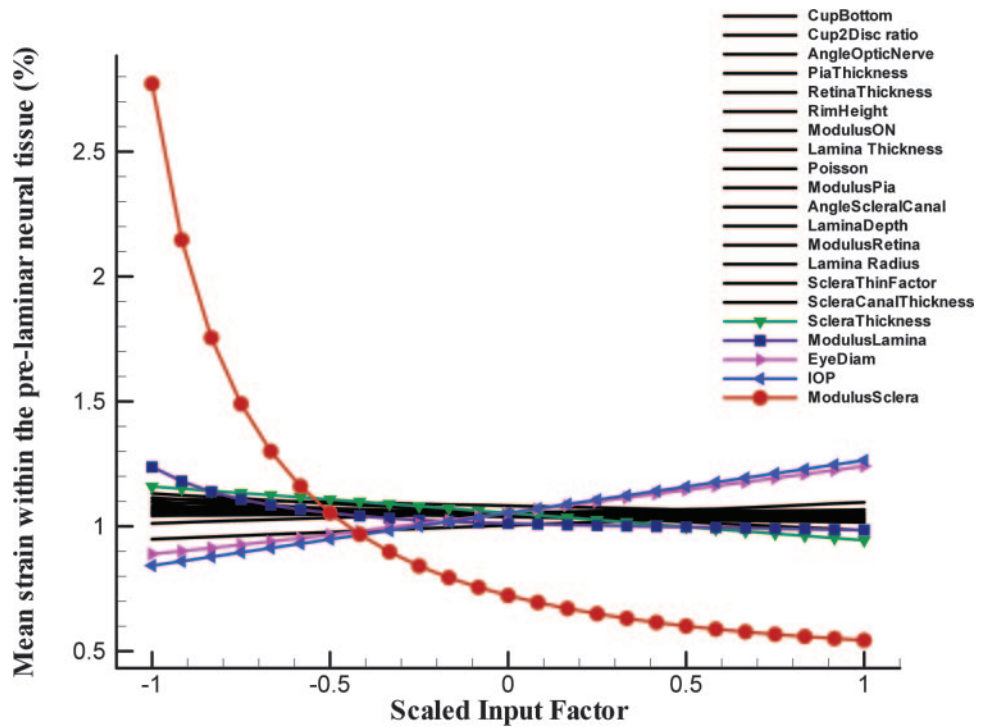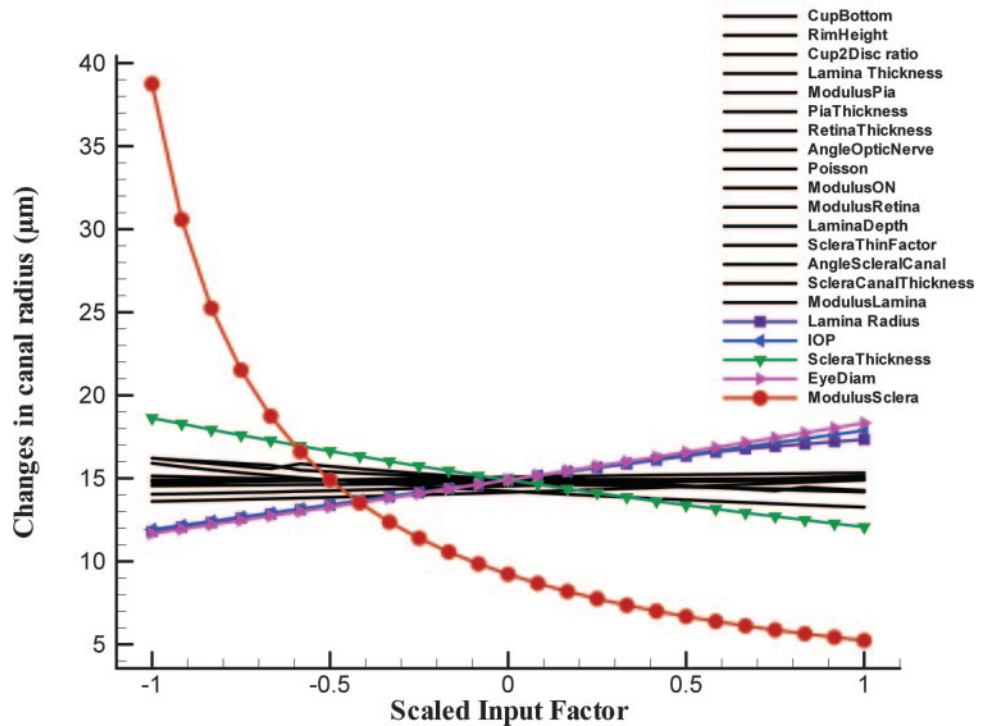
FIGURE 4. Effects of all input factors on two outcome measures: mean strain within the prelaminar neural tissue (*top*) and scleral canal radius (*bottom*). *Steep lines* represent large factor effects on the outcome measure. Factors in the legend are ordered by relative response, from smallest to largest. The five most important factors for the mean strain within the prelaminar neural tissue were (with relative response in parentheses): the modulus sclera (51%), IOP (10%), eye radius (8%), modulus lamina (6%), and scleral thickness (5%), which together account for 75% of the effects. For the changes in canal radius, the five most important factors were modulus sclera (48%), eye radius (9%), scleral thickness (9%), IOP (9%), and lamina radius (8%), which together account for 83% of the effects. The effects of the least important 16 input factors are shown as *lines without symbols.* Although it is not possible to tell the factors apart, it is clear that their effects are limited. To allow comparison of various factors on the same plot, the *x*-axis shows each input factor value linearly scaled from its minimum value (−1) to its maximum value (+1).

that no factor within the five most influential for any group was within the five least influential for any other group. Similarly, no factor that was within the five least influential factors for one group was within the five most influential for any other group. Of special interest is the outcome measure group labeled "observable" formed by cup-to-disc ratio, cup depth, and scleral canal radius, for which laminar modulus and thickness were not as influential as for other groups, whereas canal radius and scleral shell thickness has a strong influence. Interesting as well are the input factors for scleral shell thickness and pial modulus. Whereas the former was influential in all

groupings, except those of stress outcome measures, the latter shows the opposite, being only within the five most influential for the stress outcome measure groups. This difference in influence is probably the result of the large relative response of peak and mean stress within the pia to pial modulus, as can be seen in Columns 15 and 20 on the left side of Figure 5.

DISCUSSION

The goal of this study was to determine which input factors have the largest influence on ONH biomechanics. This infor-
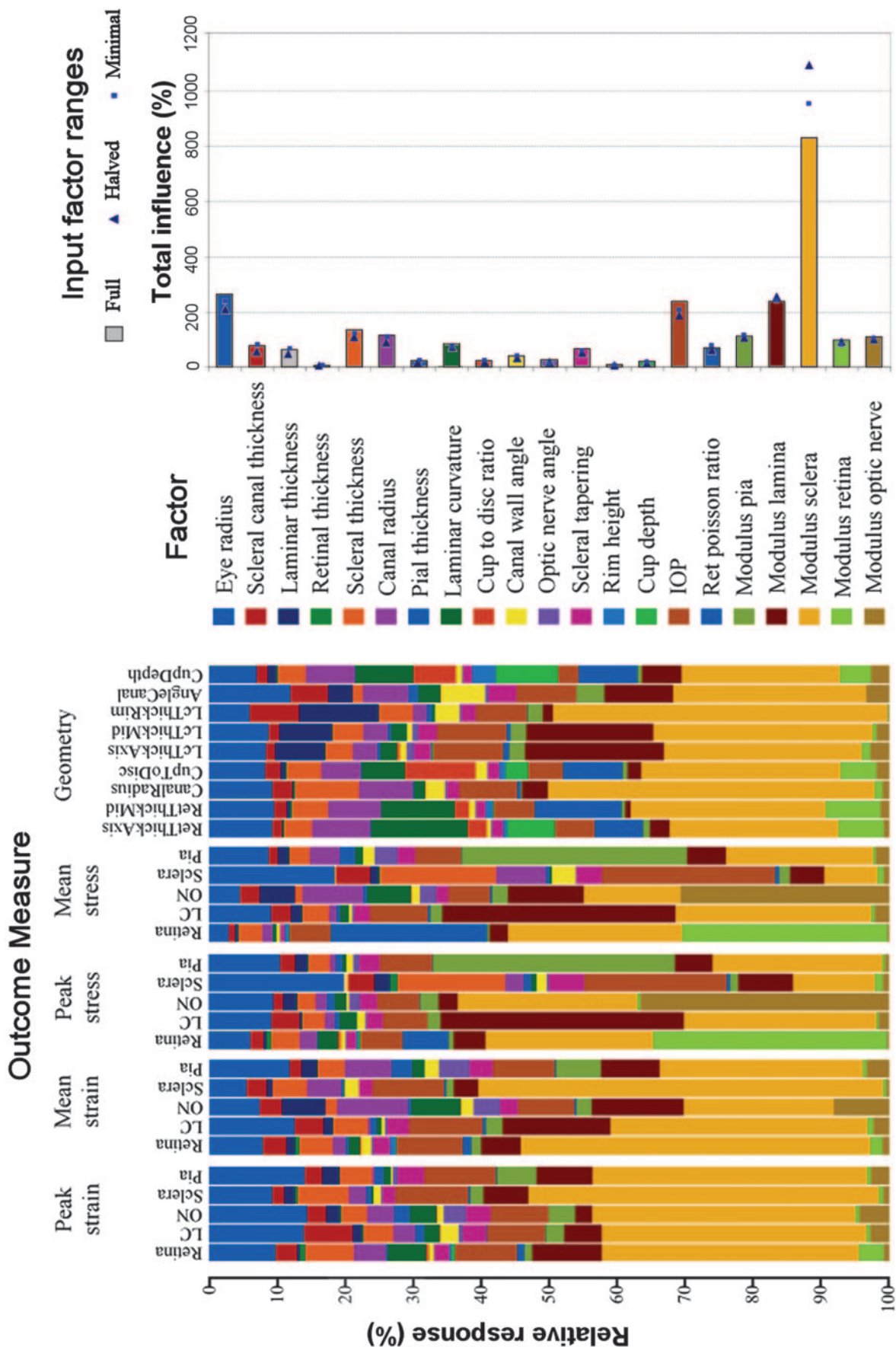
FIGURE 5. *Left:* relative response of all outcome measures to variations in all input factors. Each column corresponds to an outcome measure, colored according to the fraction of its total response resulting from variations in the input factors listed on the *right.* The order of the input factors is the same in all columns, starting from a *blue* eye radius on *top* to the *brown* modulus optic nerve at the *bottom.* All factors are plotted; however, if their effect on the outcome measure (i.e., the outcome measure relative response to the factor) is small, it may not be easily distin-guished. Larger regions of one color indicate that the input factor has a strong influence on the outcome measure. For example, variations in the modulus sclera (*orange sections*) contributed approximately 35% of the total response of the changes in mean strain within the LC (seventh column from the left). *Right:* total influences computed over all outcome measures for three different factor range conditions: full (*bars*), halved (*triangles*), and minimal (*squares*). Longer *bars* represent larger influence of the input factor over all outcome measures.

mation is valuable in three ways: It will help to guide future modeling studies; it will help to focus future experimental measurements of ONH biomechanical properties; and it may eventually provide insights into why some individuals tolerate elevated intraocular pressure better than others.

The main conclusion of this work is that the stiffness of the sclera was by far the most influential input factor. This conclusion was remarkably robust, holding true across a wide spectrum of outcome measures and for different ranges of the input factors. It is perhaps initially counterintuitive that scleral mechanical properties should have such a large influence on ONH biomechanics. This can best be understood by recalling that the sclera is the main load-bearing tissue within the eye, and therefore plays a central role in maintaining the mechanical integrity of the pressurized eye. If the stiffness of the sclera changes, the amount of deformation that it experiences at a given level of IOP also changes. Because the other ONH tissues are relatively compliant compared with the sclera, they tend to get carried along by the sclera as it deforms (i.e., scleral deformations are transmitted to all ONH tissues). Consequently, anything that changes the response of the sclera to IOP (such as scleral stiffness) has a large influence on ONH biomechanical behavior. These findings strongly suggest that scleral biomechanical properties, particularly those of the peripapillary sclera, may play an important role in the biomechanics of glaucomatous optic neuropathy.

It is very important to point out that our predictions indicate that scleral properties have the largest effect when the sclera is more compliant (see Fig. 3). Reported values of scleral stiffness vary considerably (Table 1), and to the best of our knowledge, the lowest reported value in humans is 1.8 MPa, which is slightly higher than the minimum level of 1 MPa used in this study. That means that the absolute magnitude of the sensitivity to scleral stiffness that we report is probably an overestimate. However, even accounting for this fact, scleral stiffness is still the most influential parameter we investigated; for example, the computations in which we used the minimum range of parameters, in which parameters varied by just a small amount around their baseline values, showed that scleral stiffness had by far the largest influence (Fig. 5; right). It is interesting that the minimum reported value for human scleral stiffness is right in the region where changes in scleral effects begin to be have the most effect. This reinforces our belief that we require better measurements of scleral biomechanical properties in the human eye, and how these values vary in the population, similar to the measurements performed in rabbits and monkeys by Downs and colleagues.[14,15,34,37,38,53]

The importance of scleral biomechanical properties is particularly interesting in the context of the Ocular Hypertension Treatment Study which found that central corneal thickness was an independent risk factor for the development of glaucomatous optic neuropathy,[26,27] although a recent article calls into question some of these conclusions.[9] Perhaps central corneal thickness is a surrogate measure for some essential biomechanical property or properties of the sclera. If true, this could explain why central corneal thickness, independent of corrected IOP, was associated with the risk of development of glaucomatous optic neuropathy.

Scleral stiffness was not the only influential input factor. IOP, eye globe radius, LC stiffness, scleral shell thickness, and scleral canal radius all showed appreciable influence across broad ranges of outcome measures. Scleral geometric factors (globe radius, scleral thickness) influence ONH biomechanics in a similar way to scleral stiffness, through the deformation transmitted to the peripheral ONH. This is consistent with a report by Bellezza et al.,[6] who proposed increases in IOP-related tissue stresses with increased neural canal size (corre-

sponding here to the LC radius) and peripapillary sclera thinning. Increased scleral compliance occurs, for example, in myopia, either because of scleral thinning[54] or due to alterations to the scleral extracellular matrix,[55,56] which could help explain the higher incidence of glaucomatous optic nerve damage in highly myopic eyes at a given IOP.[28,57] Increased scleral deformations may also affect blood flow through the posterior ciliary arteries,[1] also with possible harmful effects on neural tissue. This study suggests that the LC is a high-strain region, even if there is no stiffness mismatch between the LC and peripapillary sclera, contrary to previous suggestions.[3] This is because compliance depends both on biomechanical and geometric properties (e.g., thickness).

Our models predict that the specifics of the shape of the cup have a limited effect on strains in ONH tissues, as evidenced by the low influence of cup-to-disc ratio, cup depth, and peripapillary rim height across the outcome measures and input factor ranges.

Limitations

This study is subject to certain limitations. First, the effects of input factor variations were only tested independently by altering input factors one-by-one from an assumed baseline model. However, it is possible that there are interactions between the various input factors. For example, we might expect the importance of prelaminar neural tissue compressibility to increase as prelaminar neural stiffness decreases. Furthermore, two or more input factors could be correlated with one another in vivo; for example, thinner scleras could tend to have higher stiffness as a compensatory mechanism. Our approach cannot discover such interactions, should they exist. Further work is needed to investigate the effects of such interactions, but is probably premature at the present time without a more robust experimental data set of biomechanical properties to draw upon.

Second, our choice of outcome measures, their groupings and input factor ranges, although motivated by our understanding of the biology of the ONH, are somewhat arbitrary. This is particularly important for the more influential factors, like scleral stiffness. Fortunately, it was found that input factor rankings computed using full, half, or minimal ranges, and for various groups of outcome measures were surprisingly consistent. This suggests that our conclusions are robust.

Third, our models ignored long-term remodeling processes. As such, they incorporate only the acute (passive) deformation of the tissue to a step change in IOP. Our conclusions should therefore only be interpreted as giving insight during the early stages of glaucoma, before significant connective tissue remodeling occurs. It is clear that remodeling, which can for example lead to significant changes in the shape of the cup, is an important part of glaucomatous disease as it develops.[58–60]

Fourth, our models were based on a simplified axisymmetric geometry, and therefore they do not completely reflect the complex three-dimensional architecture of the ONH region,[5] which could affect the mechanical interactions between the constituent tissues. In addition, the ONH geometry may differ between individuals in more complex ways that can be captured by the input factors considered. For example, the canal wall shape may vary in ways that cannot be expressed by an angle and thickness. Efforts are already under way to address these limitations by developing individual-specific models that reproduce the details of the anatomy of an individual human ONH.[8] An important aspect of this interindividual variation will be to incorporate more accurate constitutive models of the connective tissue in the ONH region. For example, the effects of collagen fiber orientation in the peripapillary sclera could be important in influencing peripapillary scleral biomechanics.

Finally, we have assumed that all the tissues are biomechanically linear, isotropic, and homogeneous. Further work is needed to include the effects of material nonlinearity and nonhomogeneity in the models. Again, this is likely somewhat premature, given our state of knowledge about the biomechanical properties of the relevant constituent tissues within the ONH.

Summary

The complexity of ONH anatomy and material properties, combined with the variability between individuals and within an individual over a lifetime make this a difficult region to understand biomechanically. However, if as reported herein, relatively few factors account for most of the biomechanical effects, this greatly simplifies the problem of understanding ONH biomechanics. This study has identified these key factors, the most important of which is scleral biomechanical properties. Further study of scleral biomechanics in normal and glaucomatous eyes is indicated.

References

1. Burgoyne CF, Downs JC, Bellezza AJ, Suh JK, Hart RT. The optic nerve head as a biomechanical structure: a new paradigm for understanding the role of IOP-related stress and strain in the pathophysiology of glaucomatous optic nerve head damage. *Prog Retin Eye Res.* 2005;24:39–73.
2. Geijssen HC. *Studies on Normal Pressure Glaucoma.* Amsterdam: Kugler Publications; 1991.
3. Zeimer R. Biomechanical properties of the optic nerve head. In: Drance SM, Anderson RC, eds. *Optic Nerve in Glaucoma.* Amsterdam: Kugler Publications; 1995:107–121.
4. The AGIS Investigators. AGIS I: The Advanced Glaucoma Intervention Study (AGIS)—7. The relationship between control of intraocular pressure and visual field deterioration. *Am J Ophthalmol.* 2000;130:429–440.
5. Sigal IA, Flanagan JG, Tertinegg I, Ethier CR. Finite element modeling of optic nerve head biomechanics. *Invest Ophthalmol Vis Sci.* 2004;45:4378–4387.
6. Bellezza AJ, Hart RT, Burgoyne CF. The optic nerve head as a biomechanical structure: initial finite element modeling. *Invest Ophthalmol Vis Sci.* 2000;41:2991–3000.
7. Burgoyne CF, Downs JC, Bellezza AJ, Hart RT. Three-dimensional reconstruction of normal and early glaucoma monkey optic nerve head connective tissues. *Invest Ophthalmol Vis Sci.* 2004;45:4388–4399.
8. Sigal IA, Flanagan JG, Tertinegg I, Ethier CR. Reconstruction of human optic nerve heads for finite element modeling. *Technology and Health Care.* 2005;13:313–329.
9. Jonas JB, Stroux A, Velten I, Juenemann A, Martus P, Budde WM. Central corneal thickness correlated with glaucoma damage and rate of progression. *Invest Ophthalmol Vis Sci.* 2005;46:1269–1274.
10. Jonas JB, Mardin CY, Schlotzer-Schrehardt U, Naumann GO. Morphometry of the human lamina cribrosa surface. *Invest Ophthalmol Vis Sci.* 1991;32:401–405.
11. Olsen TW, Aaberg SY, Geroski DH, Edelhauser HF. Human sclera: thickness and surface area. *Am J Ophthalmol.* 1998;125:237–241.
12. Jonas JB, Berenshtein E, Holbach L. Anatomic relationship between lamina cribrosa, intraocular space, and cerebrospinal fluid space. *Invest Ophthalmol Vis Sci.* 2003;44:5189–5195.
13. Jonas JB, Berenshtein E, Holbach L. Lamina cribrosa thickness and spatial relationships between intraocular space and cerebrospinal fluid space in highly myopic eyes. *Invest Ophthalmol Vis Sci.* 2004;45:2660–2665.
14. Downs JC, Ensor ME, Bellezza AJ, Thompson HW, Hart RT, Burgoyne CF. Posterior scleral thickness in perfusion-fixed normal and early-glaucoma monkey eyes. *Invest Ophthalmol Vis Sci.* 2001;42:3202–3208.
15. Downs JC, Blidner RA, Bellezza AJ, Thompson HW, Hart RT, Burgoyne CF. Peripapillary scleral thickness in perfusion-fixed normal monkey eyes. *Invest Ophthalmol Vis Sci.* 2002;43:2229–2235.
16. Jonas JB, Holbach L. Central corneal thickness and thickness of the lamina cribrosa in human eyes. *Invest Ophthalmol Vis Sci.* 2005;46:1275–1279.
17. Quigley HA, Hohman RM, Addicks EM, Massof RW, Green WR. Morphologic changes in the lamina cribrosa correlated with neural loss in open-angle glaucoma. *Am J Ophthalmol.* 1983;95:673–691.
18. Quigley HA, Brown AE, Morrison JD, Drance SM. The size and shape of the optic disc in normal human eyes. *Arch Ophthalmol.* 1990;108:51–57.
19. Bowd C, Weinreb RN, Lee B, Emdadi A, Zangwill LM. Optic disk topography after medical treatment to reduce intraocular pressure. *Am J Ophthalmol.* 2000;130:280–286.
20. Bowd C, Weinreb RN, Williams JM, Zangwill LM. The retinal nerve fiber layer thickness in ocular hypertensive, normal and glaucomatous eyes with optical coherence tomography. *Arch Ophthalmol.* 2000;118:22–26.
21. Jonas JB, Budde WM. Diagnosis and pathogenesis of glaucomatous optic neuropathy: morphological aspects. *Prog Retin Eye Res.* 2000;19:1–40.
22. Quigley HA, Addicks EM. Regional differences in the structure of the lamina cribrosa and their relation to glaucomatous optic nerve damage. *Arch Ophthalmol.* 1981;99:137–143.
23. Jonas JB, Gusek GC, Guggenmoos-Holzmann I, Naumann GO. Size of the optic nerve scleral canal and comparison with intravital determination of optic disc dimensions. *Graefes Arch Clin Exp Ophthalmol.* 1988;226:213–215.
24. Jonas JB, Budde WM, Nemeth J, Grundler AE, Mistlberger A, Hayler JK. Central retinal vessel trunk exit and location of glaucomatous parapapillary atrophy in glaucoma. *Ophthalmology.* 2001;108:1059–1064.
25. Ikram MK, Borger PH, Assink JJ, Jonas JB, Hofman A, de Jong PT. Comparing ophthalmoscopy, slide viewing, and semiautomated systems in optic disc morphometry. *Ophthalmology.* 2002;109:486–493.
26. Herndon LW, Weizer JS, Stinnett SS. Central corneal thickness as a risk factor for advanced glaucoma damage. *Arch Ophthalmol.* 2004;122:17–21.
27. Gordon MO, Beiser JA, Brandt JD, et al. The Ocular Hypertension Treatment Study: baseline factors that predict the onset of primary open-angle glaucoma. *Arch Ophthalmol.* 2002;120:714–720.
28. Nomura H, Ando F, Niino N, Shimokata H, Miyake Y. The relationship between intraocular pressure and refractive error adjusting for age and central corneal thickness. *Ophthalmic Physiol Opt.* 2004;24:41–45.
29. Battaglioli JL, Kamm RD. Measurements of the compressive properties of scleral tissue. *Invest Ophthalmol Vis Sci.* 1984;25:59–65.
30. Uchio E, Ohno S, Kudoh J, Aoki K, Kisielewicz LT. Simulation model of an eyeball based on finite element analysis on a supercomputer. *Br J Ophthalmol.* 1999;83:1106–1111.
31. Brands DWA. *Predicting Brain Mechanics during Closed Head Impact*: *Numerical and Constitutive Aspects.* Technishe Universiteit Eindhoven, 2002. Doctoral thesis.
32. Kleiven S. *Finite Element Modeling of the Human Head.* Stockholm, Sweden: Department of Aeronautics, Royal Institute of Technology; 2002. Doctoral thesis.
33. Zhivoderov NN, Zavalishin NN, Neniukov AK. Mechanical properties of the dura mater of the human brain (in Russian). *Sud Med Ekspert.* 1983;26:36–37.
34. Bellezza AJ. *Biomechanical Properties of the Normal and Early Glaucomatous Optic Nerve Head: an Experimental and Computational Study Using the Monkey Model.* New Orleans, LA: Tulane University, Department of Biomedical Engineering; 2002. Doctoral thesis.
35. Edwards ME, Good TA. Use of a mathematical model to estimate stress and strain during elevated pressure induced lamina cribrosa deformation. *Curr Eye Res.* 2001;23:215–225.
36. Spoerl E, Boehm AG, Pillunat LE. The influence of various substances on the biomechanical behavior of lamina cribrosa and peripapillary sclera. *Invest Ophthalmol Vis Sci.* 2005;46:1286–1290.

37. Downs JC, Suh JK, Thomas KA, Bellezza AJ, Burgoyne CF, Hart RT. Viscoelastic characterization of peripapillary sclera: material properties by quadrant in rabbit and monkey eyes. *J Biomech Eng.* 2003;125:124–131.

38. Downs JC, Suh JK, Thomas KA, Bellezza AJ, Hart RT, Burgoyne CF. Viscoelastic material properties of the peripapillary sclera in normal and early-glaucoma monkey eyes. *Invest Ophthalmol Vis Sci.* 2005;46:540–546.

39. Friberg TR, Lace JW. A comparison of the elastic properties of human choroid and sclera. *Exp Eye Res.* 1988;47:429–436.

40. Kobayashi AS, Woo SL, Lawrence C, Schlegel WA. Analysis of the corneo-scleral shell by the method of direct stiffness. *J Biomech.* 1971;4:323–330.

41. Siegwart JTJ, Norton TT. Regulation of the mechanical properties of tree shrew sclera by the visual environment. *Vision Res.* 1999; 39:387–407.

42. Smolek M. Elasticity of the bovine sclera measured with real-time holographic interferometry. *Am J Optom Physiol Opt.* 1988;65: 653–660.

43. Woo SL, Kobayashi AS, Schlegel WA, Lawrence C. Nonlinear material properties of intact cornea and sclera. *Exp Eye Res.* 1972; 14:29–39.

44. Woo SL, Kobayashi AS, Lawrence C, Schlegel WA. Mathematical model of the corneo-scleral shell as applied to intraocular pressure-volume relations and applanation tonometry. *Ann Biomed Eng.* 1972;1:87–98.

45. Chang GL, Hung TK, Feng WW. An in-vivo measurement and analysis of viscoelastic properties of the spinal cord of cats. *J Biomech Eng.* 1988;110:115–122.

46. Guillaume A, Osmont D, Gaffie D, Sarron JC, Quandieu P. Effects of perfusion on the mechanical behavior of the brain-exposed to hypergravity. *J Biomech.* 1997;30:383–389.

47. Jones IL, Warner M, Stevens JD. Mathematical modelling of the elastic properties of retina: a determination of Young's modulus. *Eye.* 1992;6:556–559.

48. Metz H, McElhaney J, Ommaya AK. A comparison of the elasticity of live, dead, and fixed brain tissue. *J Biomech.* 1970;3:453–458.

49. Miller K. Constitutive model of brain tissue suitable for finite element analysis of surgical procedures. *J Biomech.* 1999;32:531–537.

50. Ozawa H, Matsumoto T, Ohashi T, Sato M, Kokubun S. Comparison of spinal cord gray matter and white matter softness: measurement by pipette aspiration method. *J Neurosurg.* 2001;95:221–224.

51. Morgan WH, Chauhan BC, Yu DY, Cringle SJ, Alder VA, House PH. Optic disc movement with variations in intraocular and cerebrospinal fluid pressure. *Invest Ophthalmol Vis Sci.* 2002;43:3236–3242.

52. Cook RD. *Finite Element Modeling for Stress Analysis.* New York: John Wiley & Sons, Inc.; 1995.

53. Burgoyne CF, Quigley HA, Thompson HW, Vitale S, Varma R. Measurement of optic disc compliance by digitized image analysis in the normal monkey eye. *Ophthalmology.* 1995;102:1790–1799.

54. Phillips JR, McBrien NA. Form deprivation myopia: elastic properties of sclera. *Ophthalmic Physiol Opt.* 1995;15:357–362.

55. McBrien NA, Cornell LM, Gentle A. Structural and ultrastructural changes to the sclera in a mammalian model of high myopia. *Invest Ophthalmol Vis Sci.* 2001;42:2179–2187.

56. McBrien NA, Gentle A. Role of the sclera in the development and pathological complications of myopia. *Prog Retin Eye Res.* 2003; 22:307–338.

57. Mitchell P, Hourihan F, Sandbach J, Wang JJ. The relationship between glaucoma and myopia: the Blue Mountains Eye Study. *Ophthalmology.* 1999;106:2010–2015.

58. Hernandez MR. The optic nerve head in glaucoma: role of astrocytes in tissue remodeling. *Prog Retin Eye Res.* 2000;19:297–321.

59. Hernandez MR, Andrzejewska WM, Neufeld AH. Changes in the extracellular matrix of the human optic nerve head in primary open-angle glaucoma. *Am J Ophthalmol.* 1990;109:180–188.

60. Morrison JC, Dorman-Pease ME, Dunkelberger GR, Quigley HA. Optic nerve head extracellular matrix in primary optic atrophy and experimental glaucoma. *Arch Ophthalmol.* 1990;108:1020–1024.